Universitat de les Illes Balears

Facultat de Ciències

Memòria del Treball de Fi de Grau

Magnetohydrodynamic waves in solar coronal loops

Antònia Galmés Melis

Grau de Física

Any acadèmic 2015-16

DNI de l'alumne: 41521597L

Treball tutelat per Ramón Oliver Herrero
Departament de Física

S'autoritza la Universitat a incloure aquest treball en el Repositori Institucional per a la seva consulta en accés obert i difusió en línia, amb finalitats exclusivament acadèmiques i d'investigació	Autor		Tutor	
	Sí	No	Sí	No
	X		X	

Paraules clau del treball:
Magnetohydrodynamics, waves, energy.

Acknowledgments

I wish to thank, first and foremost, my tutor, Ramón Oliver Herrero, for the help and support he has offered me. His guidance and advice have helped me to improve as a physicist and make possible the realization of this project. Moreover, I would also express my gratefulness to M. Carbonell (UIB) for providing me with Mathematica notebooks for the computation of solutions of the dispersion relation and for the calculation of primitives to some integrals with Bessel functions.

Contents

1. Introduction

The outermost part of the Sun's atmosphere is known as the solar corona (*Figure 1.1*) and is composed of plasma. All of the stellar interiors and atmospheres, gaseous nebulae, and much of the interstellar hydrogen are plasmas, which is the most abundant state of ordinary matter in the Universe.

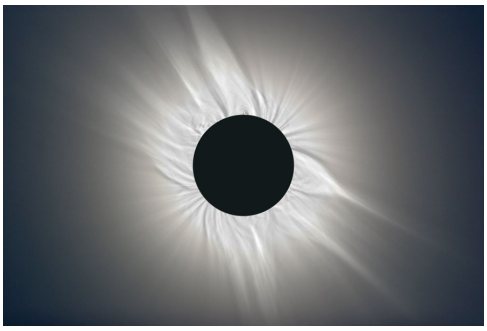

Figure 1.1: The solar corona during the total solar eclipse of March 29, 2006 (Koen van Gorp).

"A plasma is a quasineutral gas of charged and neutral particles which exhibits collective behaviour" (Chen, 1984). The movement of charge carriers can generate electric fields. Thus, it can be said that plasma is an electrically conducting fluid or gas.

On the solar disk there are regions of strong magnetic field concentrations. These regions are known as *active regions* and their distribution on the solar disk is shown *Figure 1.2*. The size of these regions varies between 50 and 100.000 Mm^2 and their lifetime, that varies up to a few months, depends on their size (Canfield, 2001). Sunspots are temporary phenomena present in active regions where the strong magnetic fields come up from within the Sun.

Coronal loops (*Figure 1.3*) are magnetic structures which can be found in active regions. Following Canfield (2001), "coronal loops outline magnetic field lines along which the ionized coronal plasma is forced to move". These structures are often associated with pairs of sunspots with opposite magnetic polarity.

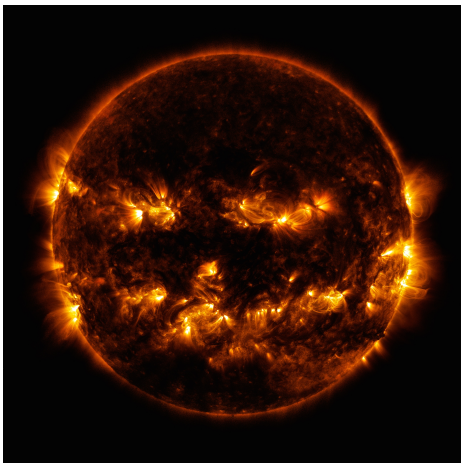

Figure 1.2: Solar active regions observed in the extreme UV band captured by NASA's Solar Dynamics Observatory.

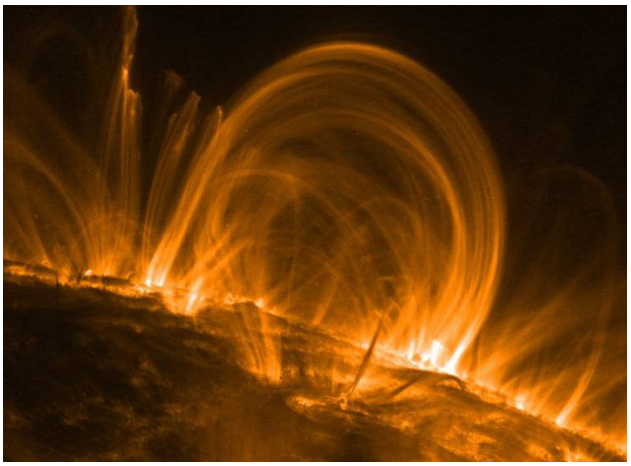

Figure 1.3: Coronal loops observed in the extreme UV band captured by NASA's Transition Region And Coronal Explorer.

Active region coronal loops are often subject to external disturbances that excite oscillations. A particularly prominent case is that of transverse oscillations: the event is usually triggered by a nearby flare and then the loop sways laterally with its feet fixed at the photosphere. *Figure 1.4* contains a schematic representation of the triggering of transverse oscillations.

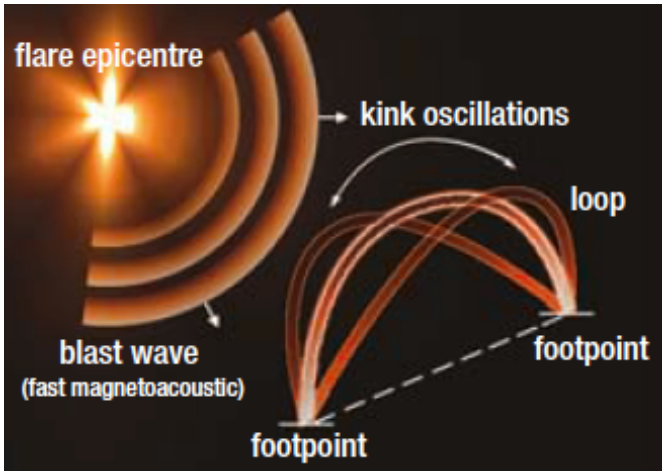

Figure 1.4: A possible mechanism for the excitation of transverse loop oscillations by a flare (from Nakariakov & Verwichte 2004).

Movie 1.1 (https://www.dropbox.com/s/ezj4zip88980fds/Movie%201.1.mov?dl=0) gives an example of one of the first detections of this phenomenon. One of the main features of these transverse loop oscillations is that the loop axis moves laterally with respect to the equilibrium position. Moreover, the oscillation is in the form of a standing wave, which implies that the triggering excites waves that propagate in both directions along the loop and that these waves interfere to produce the standing pattern.

2. MHD equations and equilibrium state

2.1 MHD equations

Magnetohydrodynamics (MHD) is the study of the motion of compressible conducting fluids in the presence of magnetic fields. For the description of the interaction between a plasma and a magnetic field it is necessary to consider the plasma as a continuous fluid.

The set of the ideal MHD equations are a combination of the electromagnetic equations (Maxwell equations and Ohm's law) and the equations of fluid mechanics (the Navier-Stokes equations for a Newtonian fluid). In order to simplify this set of equations, the MHD approximation is applied. This approximation is based on the assumption that the characteristic speeds in plasmas are much less than the speed of light (Goedbloed and Poedts, 2004; Priest, 2014).

Within this approximation, the non-relativistic ideal magnetohydrodynamics equations for the motion of plasma in the presence of a magnetic field can be written as

$$Continuity \qquad \frac{\partial \rho}{\partial t} + \nabla \cdot (\rho\, \boldsymbol{v}) = 0, \tag{2.1}$$

$$Momentum \qquad \rho \frac{D\boldsymbol{v}}{Dt} = -\nabla p + \frac{1}{\mu_0}(\nabla \times \boldsymbol{B}) \times \boldsymbol{B}, \tag{2.2}$$

$$Induction \qquad \frac{\partial \boldsymbol{B}}{\partial t} = \nabla \times (\boldsymbol{v} \times \boldsymbol{B}), \tag{2.3}$$

$$Solenoidal \qquad \nabla \times \boldsymbol{B} = 0. \tag{2.4}$$

To model the solar corona using the MHD equations it is important to define the parameter β that gives the relative importance of the plasma pressure (p) to the magnetic pressure ($B^2/2\mu_0$) forces. It is defined as

$$\beta = \frac{p}{B^2/2\mu_0}. \tag{2.5}$$

There are two limit cases:

- $\beta \ll 1$: the magnetic field dominates the dynamics of the plasma over fluid dynamics.
- $\beta \gg 1$: the magnetic forces are negligible and the motion of the plasma is determined by the fluid dynamics.

The particular case where $\beta = 0$ is known as cold plasma, which is characterized by $\nabla p = \mathbf{0}$. In this case, the momentum equation (2.2) can be simplified as

$$\rho \frac{D\boldsymbol{v}}{Dt} = \frac{1}{\mu_0}(\nabla \times \boldsymbol{B}) \times \boldsymbol{B}. \tag{2.6}$$

In addition, the displacement of a plasma element and the velocity are related by

$$\boldsymbol{v} = \frac{D\boldsymbol{\xi}}{Dt} = \left(\frac{\partial}{\partial t} + \boldsymbol{v} \cdot \nabla\right)\boldsymbol{\xi}. \tag{2.7}$$

Then, the momentum equation can be written in terms of the displacement vector as follows

$$\rho \frac{D^2\boldsymbol{\xi}}{Dt^2} = +\frac{1}{\mu_0}(\nabla \times \boldsymbol{B}) \times \boldsymbol{B}. \tag{2.8}$$

2.2. Equilibrium

In order to model MHD waves in solar coronal loops we will consider the loop as a cylinder of radius a with a constant magnetic field $\boldsymbol{B_0}$ applied in the z direction (*Figure 2.1*). This uniform magnetic field is present both inside the coronal loop and its environment. Furthermore, we will assume that the equilibrium density, denoted by ρ_0, is uniform inside and outside the cylinder, with values ρ_i and ρ_e, respectively. From observations, the condition $\rho_i > \rho_e$ is satisfied.

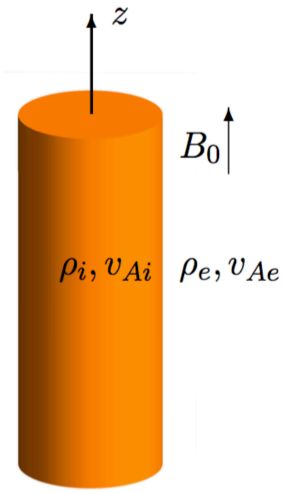

Figure 2.1: Representation of a coronal loop as a straight cylinder, i.e., with its curvature being neglected.

The Alfvén speed is defined as

$$v_A^2 = \frac{B_0}{\mu_0 \rho_0}. \tag{2.9}$$

Depending on the value of the density ρ_0, we will have an internal, v_{Ai}, or external, v_{Ae}, Alfvén speed, as shown in *Figure 2.1*.

Due to the definition (2.9), the internal and external densities and Alfvén speeds are related through the following equation

$$\rho_i \, v_{Ai}^2 = \rho_e \, v_{Ae}^2 = \rho_0 \, v_A^2, \tag{2.10}$$

where ρ_0 and v_A implicitly contain the dependence of the density and Alfvén speed with respect to the distance to the cylinder axis, r.

3. Linear MHD waves in a magnetic cylinder

In this section we present the equations that describe MHD waves propagating along a coronal loop modeled as a magnetic cylinder. We also obtain expressions for the wave frequency and the eigenfunctions, and include some plots to help interpret the physical nature of these solutions. The material in this section is partly based on Ruderman and Erdelyi (2009).

3.1. Linear wave equations

We consider a coronal loop in static equilibrium, modelled as a straight magnetic cylinder whose density and magnetic field are given in section 2. We now consider perturbations about the equilibrium state, so that the perturbed variables are:

- Magnetic field: $\boldsymbol{B}(\boldsymbol{r},t) = \boldsymbol{B_0}(\boldsymbol{r}) + \boldsymbol{B_1}(\boldsymbol{r},t),$ (3.1)
- Density: $\rho(\boldsymbol{r},t) = \rho_0(\boldsymbol{r}) + \rho_1(\boldsymbol{r},t),$ (3.2)
- Velocity: $\boldsymbol{v}(\boldsymbol{r},t) = \boldsymbol{v_0}(\boldsymbol{r}) + \boldsymbol{v_1}(\boldsymbol{r},t),$ (3.3)
- Displacement vector: $\boldsymbol{\xi}(\boldsymbol{r},t) = \boldsymbol{\xi_0}(\boldsymbol{r}) + \boldsymbol{\xi_1}(\boldsymbol{r},t),$ (3.4)

with $\boldsymbol{v_0}(\boldsymbol{r},t) = \boldsymbol{\xi_0}(\boldsymbol{r},t) = \boldsymbol{0}$.

Then all these perturbed quantities can be introduced in the MHD equations. In the derivation that follows we will assume that perturbations are much smaller than their corresponding equilibrium values, i.e., $|\boldsymbol{B_0}| \gg |\boldsymbol{B_1}|$ and $\rho_0 \gg \rho_1$. This allows us to neglect the products of perturbations.

- Displacement vector (2.7):

$$\boldsymbol{v} = \frac{D\boldsymbol{\xi}}{Dt} = \left(\frac{\partial}{\partial t} + \boldsymbol{v}\cdot\nabla\right)\boldsymbol{\xi} \approx \frac{\partial \boldsymbol{\xi}}{\partial t}. \tag{3.5}$$

- Continuity equation (2.1):

$$\frac{\partial}{\partial t}(\rho_0 + \rho_1) = -\nabla\cdot\left((\rho_0 + \rho_1)\,\boldsymbol{v}\right). \tag{3.6}$$

  Considering that the equilibrium density is much bigger than the perturbed density and independent of time, the continuity equation reduces to

$$\frac{\partial \rho_1}{\partial t} = -\nabla\cdot(\rho_0\,\boldsymbol{v}), \tag{3.7}$$

and using the definition of the velocity (3.5)

$$\frac{\partial \rho_1}{\partial t} = -\nabla \cdot \left(\rho_0 \frac{\partial \boldsymbol{\xi}}{\partial t}\right). \tag{3.8}$$

- Momentum equation (2.8):

$$(\rho_0 + \rho_1)\frac{\partial^2 \boldsymbol{\xi}}{\partial t^2} = \frac{1}{\mu_0}\big(\nabla\times(\boldsymbol{B_0} + \boldsymbol{B_1})\big)\times(\boldsymbol{B_0} + \boldsymbol{B_1}). \tag{3.9}$$

The magnetic field in equilibrium has the general form $\boldsymbol{B_0} = B_0\,\hat{e}_z$. In addition, the magnetic field and density perturbation terms are much smaller than the equilibrium terms, $|\boldsymbol{B_0}| \gg |\boldsymbol{B_1}|$ and $\rho_0 \gg \rho_1$, and products of perturbations are negligible. Then the above expression can be simplified to

$$\rho_0 \frac{\partial^2 \boldsymbol{\xi}}{\partial t^2} = -\frac{1}{\mu_0}\boldsymbol{B_0}\times(\nabla\times\boldsymbol{B_1}). \tag{3.10}$$

We next rewrite this formula with the help of the relation $\nabla(\boldsymbol{A}\cdot\boldsymbol{B}) = (\boldsymbol{A}\cdot\nabla)\cdot\boldsymbol{B} + (\boldsymbol{B}\cdot\nabla)\cdot\boldsymbol{A} + \boldsymbol{A}\times(\nabla\times\boldsymbol{B}) + \boldsymbol{B}\times(\nabla\times\boldsymbol{A})$,

$$\rho_0 \frac{\partial^2 \boldsymbol{\xi}}{\partial t^2} = -\frac{1}{\mu_0}\nabla(B_0 B_z) + \frac{1}{\mu_0}(\boldsymbol{B_0}\cdot\nabla)\boldsymbol{B_1}, \tag{3.11}$$

where B_z is the z-component of $\boldsymbol{B_1}$. Finally, this equation can be expressed as

$$\rho_0 \frac{\partial^2 \boldsymbol{\xi}}{\partial t^2} = -\nabla P + \frac{1}{\mu_0}(\boldsymbol{B_0}\cdot\nabla)\boldsymbol{B_1}, \tag{3.12}$$

where the total pressure perturbation has been defined as

$$P = \frac{B_0 B_z}{\mu_0}. \tag{3.13}$$

- Induction equation (2.3):

$$\frac{\partial}{\partial t}(\boldsymbol{B_0} + \boldsymbol{B_1}) = \nabla\times\big(\boldsymbol{v}\times(\boldsymbol{B_0} + \boldsymbol{B_1})\big). \tag{3.14}$$

Using the fact that the equilibrium magnetic field is independent of time and that it is much larger than its perturbation, $|\boldsymbol{B_0}| \gg |\boldsymbol{B_1}|$, equation (3.14) leads to

$$\frac{\partial \boldsymbol{B_1}}{\partial t} = \nabla\times(\boldsymbol{v}\times\boldsymbol{B_0}). \tag{3.15}$$

This equation can be simplified using expression (3.5), the relation $\nabla\times(\boldsymbol{A}\times\boldsymbol{B}) = (\boldsymbol{B}\cdot\nabla)\cdot\boldsymbol{A} + \boldsymbol{A}\cdot(\nabla\cdot\boldsymbol{B}) - (\boldsymbol{A}\cdot\nabla)\cdot\boldsymbol{B} - \boldsymbol{B}\cdot(\nabla\cdot\boldsymbol{A})$ and the fact that the magnetic field in equilibrium has the general form $\boldsymbol{B_0} = B_0\,\hat{e}_z$,

$$\frac{\partial \boldsymbol{B_1}}{\partial t} = B_0 \frac{\partial^2 \boldsymbol{\xi}}{\partial z\, \partial t} - B_0 \left(\nabla \cdot \left(\frac{\partial \boldsymbol{\xi}}{\partial t} \right) \right) \hat{e}_z. \tag{3.16}$$

The perturbations $\boldsymbol{B_1}$ and $\boldsymbol{\xi_1}$ can be decomposed in two different components, one in the z-direction and the other one in the perpendicular direction to the z-axis

$$\boldsymbol{B_1} = \boldsymbol{B}_\perp + B_z\, \hat{e}_{\boldsymbol{z}}, \tag{3.17}$$

$$\boldsymbol{\xi} = \boldsymbol{\xi}_\perp + \xi_z\, \hat{e}_z, \tag{3.18}$$

with $\begin{cases} \boldsymbol{B}_\perp = B_r\, \hat{e}_r + B_\varphi \hat{e}_\varphi, \\ \boldsymbol{\xi}_\perp = \xi_r\, \hat{e}_r + \xi_\varphi \hat{e}_\varphi. \end{cases}$

The decomposition of equations (3.12) and (3.16) in these two components is

$$\rho_0\, \frac{\partial^2 \boldsymbol{\xi}}{\partial t^2} = -\nabla P + \frac{1}{\mu_0} (\boldsymbol{B_0} \cdot \nabla) \boldsymbol{B_1} \quad \rightarrow \quad \begin{cases} \dfrac{\partial^2 \boldsymbol{\xi}_\perp}{\partial t^2} = -\dfrac{1}{\rho_0} \nabla_\perp P + v_A^2 \dfrac{\partial^2 \boldsymbol{\xi}_\perp}{\partial z^2}, & (3.19) \\ \xi_z = 0, & (3.20) \end{cases}$$

$$\frac{\partial \boldsymbol{B_1}}{\partial t} = \mathrm{B}_0\, \frac{\partial^2 \boldsymbol{\xi}}{\partial z\, \partial t} - B_0 \left(\nabla \cdot \left(\frac{\partial \boldsymbol{\xi}}{\partial t} \right) \right) \hat{e}_z \quad \rightarrow \quad \begin{cases} \dfrac{\partial \boldsymbol{B}_\perp}{\partial t} = B_0 \dfrac{\partial^2 \boldsymbol{\xi}_\perp}{\partial z\, \partial t}, & (3.21) \\ \dfrac{\partial B_z}{\partial t} = -B_0 \left(\nabla_\perp \cdot \left(\dfrac{\partial \boldsymbol{\xi}_\perp}{\partial t} \right) \right), & (3.22) \end{cases}$$

with $\nabla_\perp = \nabla - \frac{\partial}{\partial z} \hat{e}_z$.

In the cylindrical geometry considered here, perturbed quantities have the general form

$$f(\boldsymbol{r}, t) = f_0(\boldsymbol{r}) + f_1(\boldsymbol{r}, t) = f_0(\boldsymbol{r}) + \hat{f}(r) e^{i\phi}, \tag{3.23}$$

with $\phi = -\omega t + m\varphi + kz$. Here ω is the frequency, m is the azimuthal wavenumber and k is the longitudinal wavenumber. Hence, the solutions considered here are waves that propagate along the coronal loop with wavelength $\lambda = 2\pi/k$. Equation (3.19) can be developed as

$$\omega^2 \hat{\boldsymbol{\xi}}_\perp = \frac{1}{\rho_0} \left(\frac{\partial \hat{P}}{\partial r} \hat{e}_r + \frac{1}{r} \frac{\partial P}{\partial \varphi} \hat{e}_\varphi \right) + v_A^2\, k^2\, \hat{\boldsymbol{\xi}}_\perp. \tag{3.24}$$

The radial component of this equation is

$$\omega^2 \hat{\xi}_r = \frac{1}{\rho_0} \frac{\partial \hat{P}}{\partial r} + v_A^2\, k^2 \hat{\xi}_r. \tag{3.25}$$

Defining

$$k_r^2 = \frac{\omega^2 - k^2\, v_A^2}{v_A^2}, \tag{3.26}$$

we end up with

$$\hat{\xi}_r = \frac{1}{\rho_0\, v_A^2\, k_r^2}\, \frac{\partial \hat{P}}{\partial r}. \tag{3.27}$$

The azimuthal component of equation (3.24) is

$$\omega^2 \hat{\xi}_\varphi = \frac{1}{\rho_0} \frac{1}{r} \frac{\partial \hat{P}}{\partial \varphi} + v_A^2\, k^2 \hat{\xi}_\varphi, \tag{3.28}$$

so that

$$\hat{\xi}_\varphi = \frac{im}{r\, \rho_0\, v_A^2\, k_r^2}\, \hat{P}. \tag{3.29}$$

Using the general form of equation (3.23) for the perturbed quantities B_z and $\boldsymbol{\xi}_\perp$, then equation (3.22) can be written as follows

$$\hat{B}_z = -B_0 \left(\nabla_\perp \cdot \hat{\boldsymbol{\xi}}_\perp\right). \tag{3.30}$$

We can find an expression for the total pressure using equations (3.13) and (3.22)

$$\hat{P} = -\rho_0\, v_A^2\, \nabla_\perp \cdot \hat{\boldsymbol{\xi}}_\perp. \tag{3.31}$$

Using the radial and azimuthal components of the displacement vectors (3.27) and (3.29), the above expression can be written as

$$\hat{P} = -\rho_0\, v_A^2 \left(\frac{1}{r}\frac{\partial}{\partial r}\left(r\, \frac{1}{\rho_0\, v_A^2\, k_r^2}\frac{\partial \hat{P}}{\partial r}\right) + \frac{1}{r}\frac{\partial}{\partial \varphi}\left(\frac{im}{r\, \rho_0\, v_A^2\, k_r^2}\, \hat{P}\right)\right). \tag{3.32}$$

So we finally obtain the following ordinary differential equation for $\hat{P}(r)$

$$\frac{d^2\hat{P}}{dr^2} + \frac{1}{r}\frac{d\hat{P}}{dr} + \left(k_r^2 - \frac{m^2}{r^2}\right)\hat{P} = 0. \tag{3.33}$$

3.2. Eigenmodes

Depending on the sign of k_r^2, equation (3.33) is Bessel's differential equation ($k_r^2 > 0$) or the modified Bessel's differential equation ($k_r^2 < 0$). Therefore, the solutions of this equation are a linear combination of Bessel functions

$$\hat{P}(r) = \begin{cases} C_1\, J_m(k_r\, r) + C_2\, Y_m(k_r\, r), & k_r^2 > 0, \quad (3.34) \\ C_3\, I_m(\kappa_r\, r) + C_4\, K_m(\kappa_r\, r), & k_r^2 < 0, \quad (3.35) \end{cases}$$

where $\kappa_r^2 = -k_r^2 = -\frac{\omega^2 - k^2\, v_A^2}{v_A^2}$ and C_1, C_2, C_3, C_4 are arbitrary constants. Furthermore, the functions $J_m(r)$, $Y_m(r)$, $I_m(r)$, $K_m(r)$ are the Bessel's and the modified Bessel's functions of first and second kind.

Since the equilibrium density is different inside and outside the cylinder, $\rho_i \neq \rho_e$, the Alfvén speed will also be different inside and outside the cylinder and, therefore, the variable k_r^2 takes the values

$$\begin{cases} k_i^2 = \dfrac{\omega^2 - k^2 v_{Ai}^2}{v_{Ai}^2} = -\kappa_i^2, & r \leq a, \quad (3.36) \\ k_e^2 = \dfrac{\omega^2 - k^2 v_{Ae}^2}{v_{Ae}^2} = -\kappa_e^2, & r > a, \quad (3.37) \end{cases}$$

Therefore, for a fixed longitudinal wavenumber, k, depending on the value of the frequency, ω, there will be three different regions, schematically represented in *Figure 3.1.*

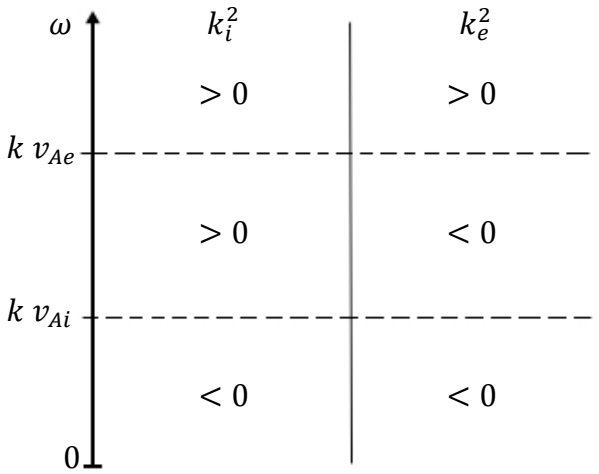

Figure 3.1: Frequency regions for different values of k_r^2.

To find the solution for $\hat{P}(r)$ in each region, the non-divergence of the pressure is imposed when $r \to 0$ and when $r \to \infty$. The pressure in each region inside and outside the cylinder is presented in *Table 3.1*

ω	$r \leq a$	$r \geq a$
$0 < \omega < k\, v_{Ai}$	$C_{3i}\, I_m(\kappa_i\, r)$	$C_{4e}\, K_m(\kappa_e\, r)$
$k\, v_{Ai} < \omega < k\, v_{Ae}$	$C_{1i}\, J_m(k_i\, r)$	$C_{4e}\, K_m(\kappa_e\, r)$
$k\, v_{Ae} < \omega$	$C_{1i}\, J_m(k_i\, r)$	$C_{1e}\, J_m(k_e\, r) + C_{2e}\, Y_m(k_e\, r)$

Table 3.1: Radial variation of the total pressure $\hat{P}(r)$, in each frequency region.

In *Table 3.1* $C_{1i}, C_{1e}, C_{2e}, C_{3i}, C_{4e}$ are arbitrary constants. To find restrictions on their value, continuity of the perturbed pressure and the radial component of the displacement vector at $r = a$ must be imposed. Each frequency region is now analysed separately.

1) For the region $0 < \omega < k\, v_{Ai}$ the continuity of $\hat{P}(r)$ and $\hat{\xi}_r(r)$ at $r = a$ implies

$$\begin{cases} C_{3i}\, I_m(\kappa_i a) = C_{4e}\, K_m(\kappa_e a), & (3.38) \\ \dfrac{-1}{\rho_i\, v_{Ai}^2\, \kappa_i} C_{3i}\, I'_m(\kappa_i a) = \dfrac{-1}{\rho_e\, v_{Ae}^2\, \kappa_e} C_{4e}\, K'_m(\kappa_e a). & (3.39) \end{cases}$$

This is a homogeneous system of linear algebraic equations for C_{3i} and C_{4e}. In order to have a non-trivial solution, its determinant must be zero. This condition leads to

$$\frac{I'_m(\kappa_i a)}{\kappa_i\, I_m(\kappa_i a)} - \frac{K'_m(\kappa_e a)}{\kappa_e\, K_m(\kappa_e a)} = 0. \quad (3.40)$$

The modified Bessel function of first kind $I_m(r)$ and its derivative $I_m{}'(r)$ are always positive. Moreover, the modified Bessel function of second kind $K_m(r)$ is positive but its derivative $K_m{}'(r)$ is negative. Thus, it is easy to prove that the equation (3.40) has no solution. In other words, the coronal loop model used here cannot support waves with $0 < \omega < k\, v_{Ai}$.

2) In the second region, $k\, v_{Ai} < \omega < k\, v_{Ae}$, the continuity constraint gives the system of equations

$$\begin{cases} C_{1i}\, J_m(k_i a) = C_{4e}\, K_m(\kappa_e a), & (3.41) \\ \dfrac{1}{\rho_i\, v_{Ai}^2\, k_i} C_{1i}\, J'_m(k_i a) = \dfrac{-1}{\rho_e\, v_{Ae}^2\, \kappa_e} C_{4e}\, K'_m(\kappa_e a), & (3.42) \end{cases}$$

This is a homogeneous system of linear algebraic equations for C_{1i} and C_{4e}. As in the previous case, its determinant must be zero. Therefore, it leads us to the following condition

$$\frac{J_m{}'(k_i a)}{k_i\, J_m(k_i a)} + \frac{K_m{}'(\kappa_e a)}{\kappa_e\, K_m(\kappa_e a)} = 0. \tag{3.43}$$

In this case, equation (3.43) has a solution, which allows one to obtain ω once m and k are imposed. This is called the dispersion relation.

3) The continuity of $\hat{P}(r)$ and $\hat{\xi}_r(r)$ at $r = a$ in the last region, $k\, v_{Ae} < \omega$, implies

$$\begin{cases} C_{1i}\, J_m(k_i a) = C_{1e}\, J_m(k_e a) + C_{2e}\, Y_m(k_e a), & (3.44) \\ \dfrac{1}{\rho_i\, v_{Ai}^2\, k_i} C_{1i}\, J'_m(k_i a) = \dfrac{1}{\rho_e\, v_{Ae}^2\, k_e} (C_{1e}\, J'_m(k_e a) + C_{2e}\, Y'_m(k_e a)), & (3.45) \end{cases}$$

In the present case we have only two equations for the three unknowns C_{1i}, C_{1e} and C_{2e}. One can then consider one of these three constants as a truly arbitrary parameter and use equations (3.44) and (3.45) to express the other two as a function of the first one. Using this procedure, one can, for example, cast C_{1i} and C_{2e} in terms of C_{1e}. Then, we obtain

$$\begin{cases} C_{1i} = \dfrac{k_i\, J'_m(k_e a)\, Y_m(k_e a) - k_i\, J_m(k_e a)\, Y'_m(k_e a)}{k_e\, J'_m(k_i a)\, Y_m(k_e a) - k_i\, J_m(k_i a)\, Y'_m(k_e a)}\, C_{1e}, & (3.46) \\ C_{2e} = \dfrac{k_i\, J_m(k_i a)\, J'_m(k_e a) - k_e\, J'_m(k_i a)\, J_m(k_e a)}{k_e\, J'_m(k_i a)\, Y_m(k_e a) - k_i\, J_m(k_i a)\, Y'_m(k_e a)}\, C_{1e}. & (3.47) \end{cases}$$

Obviously this is not the only way to write two of the three constants as functions of the third one. In fact, in *section 3.6.2* we will make a different choice.

It is worth noting that, in the present case, we do not obtain a dispersion relation. This means that, once m and k are fixed, any value of the frequency above $k\, v_{Ae}$ is a solution to the problem. For this reason, the solutions in this frequency region are called "continuous", whereas those in the range $k\, v_{Ai} < \omega < k\, v_{Ae}$ are called "discrete".

3.3. Kink mode

The preceding treatment of the linear solutions to the MHD wave equations has been done for any value of the azimuthal wavenumber, m. Transverse loop oscillations have been abundantly reported (see section 1) and for this reason we next concentrate in these events. Except for the $m = 1$ modes, all solutions leave the loop axis undisturbed and therefore only $m = 1$ waves are of interest here. These solutions deform the loop in the form of a kink (see *Figure 3.2*). When two kink waves of equal amplitude travel in

opposite directions the standing pattern of *Figure 3.3* is generated. The observed standing transverse loop oscillations are often interpreted as a standing kink wave with only two nodes, at the loop feet, and a single maximum, at the loop top. In the rest of this work we thus concentrate in the $m = 1$ case.

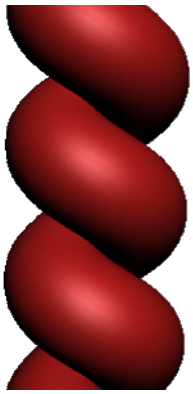

Figure 3.2: Shape of a loop disturbed by a kink wave.

Figure 3.3: Straight magnetic cylinder perturbed by two kink waves travelling in opposite directions.

3.4. Dimensionless variables and functions

To plot the results we have obtained we will use variables and functions without dimensions. To obtain dimensionless variables and functions defined in *Table 3.2* we use the following quantities: v_{Ai} (internal Alfvén speed), ρ_i (internal density) and a (tube radius).

Variables	
Length	$\bar{l} = \frac{l}{a}$
Speed	$\bar{v} = \frac{v}{v_{Ai}}$
Wavenumber	$\bar{k} = ka$
Time	$\bar{t} = t\frac{v_{Ai}}{a}$
Frequency	$\bar{\omega} = \omega\frac{a}{v_{Ai}}$

Functions	
Pressure	$\bar{P} = \frac{P}{\rho_i v_{Ai}^2}$
Magnetic field	$\bar{B} = \frac{B}{B_0}$
Energy per unit volume	$\bar{E} = \frac{E}{\rho_i v_{Ai}^2}$

Table 3.2: Dimensionless variables and functions.

3.5. Dispersion relation

We can represent the allowed frequency values with the dimensionless variables defined in *Table 3.2*. The allowed frequency values are represented in *Figure 3.4* for the density ratio $\rho_e/\rho_i = 1/4$ (which is equivalent to $v_{Ae}/v_{Ai} = 2$) and $m = 1$.

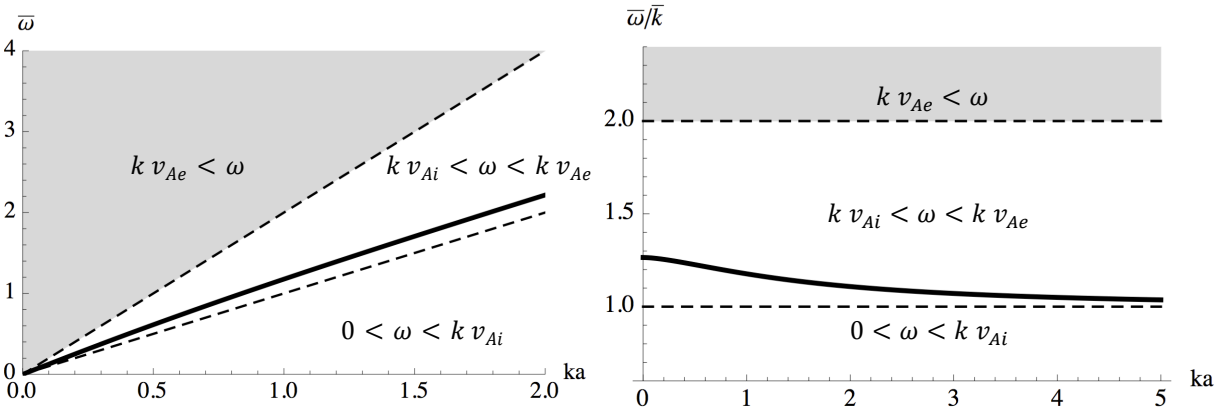

Figure 3.4: Plot of the frequency (left) and the phase velocity (right) for the various wave modes supported by a magnetic cylinder.

In *Figure 3.4* we can observe the three frequency regions, separated by dashed lines. Furthermore, in each region the different allowed frequency values are shown. As we have found in the previous subsection there cannot be waves with $0 < \omega < k\,v_{Ai}$. On the other hand, in the region $k\,v_{Ae} < \omega$ there is a continuous of solutions such that for a fixed m and k any value of the frequency above $k\,v_{Ae}$ is allowed; for this reason this area is shaded. Finally, in the central region the solution to the dispersion relation, equation (3.43), is plotted with a solid line. It is worth mentioning that the dispersion relation possesses more solutions. The one displayed in *Figure 3.4* is the fundamental mode, which is the most relevant solution since it contains the largest spatial scales and so it is the most easily excited by a perturbation. Hence, in this region, for each k there is only one allowed value for frequency given by equation (3.43).

The right panel of *Figure 3.4* is included here because observations of coronal disturbances often allow to determine the phase speed, and so this panel can be used to compare the results of the simple cylinder model with the detected phase velocities.

3.6. Eigenfunctions

In this section we will analyze the two regions that have allowed frequency values.

3.6.1. Region 1

Such as we have just described, in the first region, $k\,v_{Ai} < \omega < k\,v_{Ae}$, there is a dispersion relation (3.43) which for a fixed k and m gives us a value of frequency ω.

In order to simplify the expressions of the pressure and the displacement vector, the arbitrary constants C_{1i} and C_{4e} are defined such that the radial displacement at the loop boundary is $\hat{\xi}_r(r=a)=1$. We will obtain these two constants using the expression of the pressure (*Table 3.1*) and the definition of the radial displacement (3.27).

$$\begin{cases} C_{1i} = \dfrac{\rho_i v_{Ai}^2 k_i}{J'_m(k_i a)}, & (3.48) \\ C_{4e} = -\dfrac{\rho_e\, v_{Ae}^2\, \kappa_e}{K'_m(\kappa_e a)}. & (3.49) \end{cases}$$

Using the above constants, the pressure in this frequency region for a given k and m is

$$\hat{P}(r) = \begin{cases} \dfrac{\rho_i v_{Ai}^2 k_i}{J'_m(k_i a)}\, J_m(k_i r), & r \le a, \quad (3.50) \\ -\dfrac{\rho_e v_{Ae}^2 \kappa_e}{K'_m(\kappa_e a)}\, K_m(\kappa_e r), & r > a. \quad (3.51) \end{cases}$$

Then, the perturbed pressure (3.50 and 3.51) and the radial (3.27) and azimuthal (3.29) components of the displacement vector can be represented for fixed values of k and m. They are plotted in the following figures for the same parameter values used before, namely $\rho_e/\rho_i = 1/4$ and $m = 1$, and for two different values of k. The frequency in each case is calculated through the dispersion relation (3.43) before the eigenfunctions can be plotted.

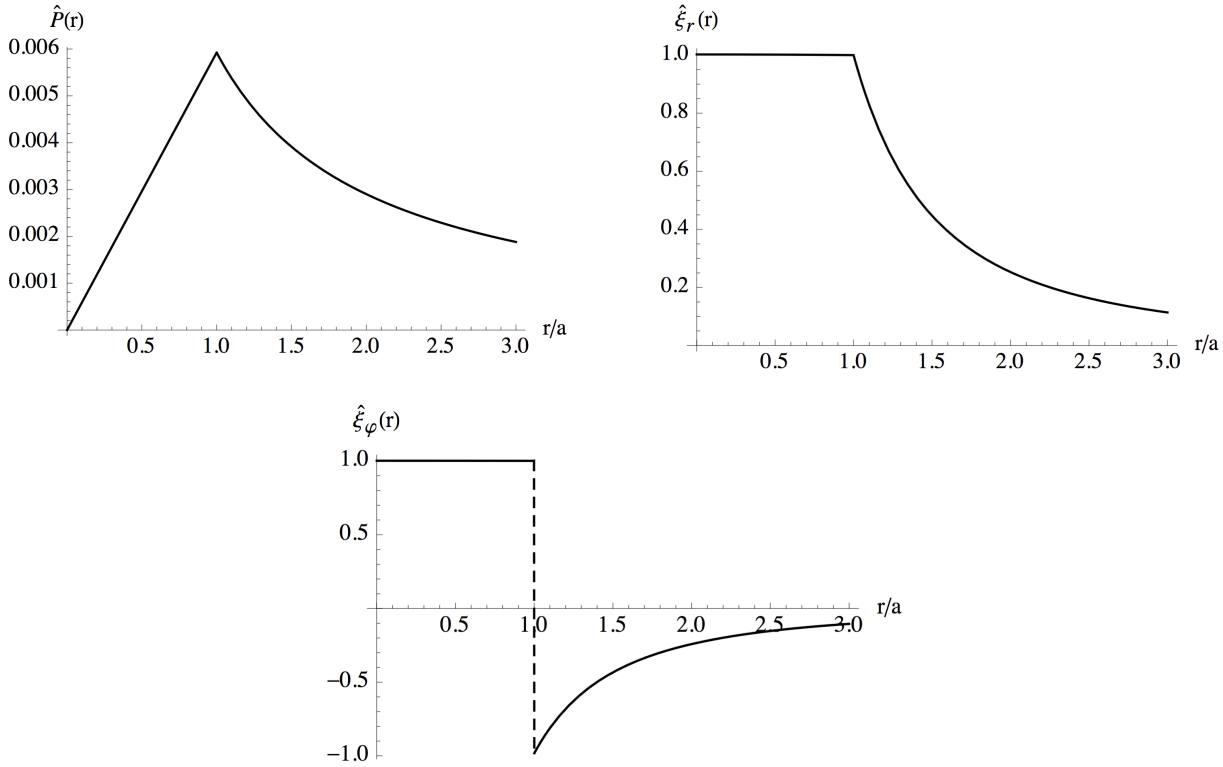

Figure 3.5: Perturbed pressure and displacement vector for ka=0.1, which corresponds to the longitudinal wavelength $\lambda = 20\pi a$. The eigenfunctions have been normalized so that the radial displacement is equal to one at the loop boundary ($r = a$).

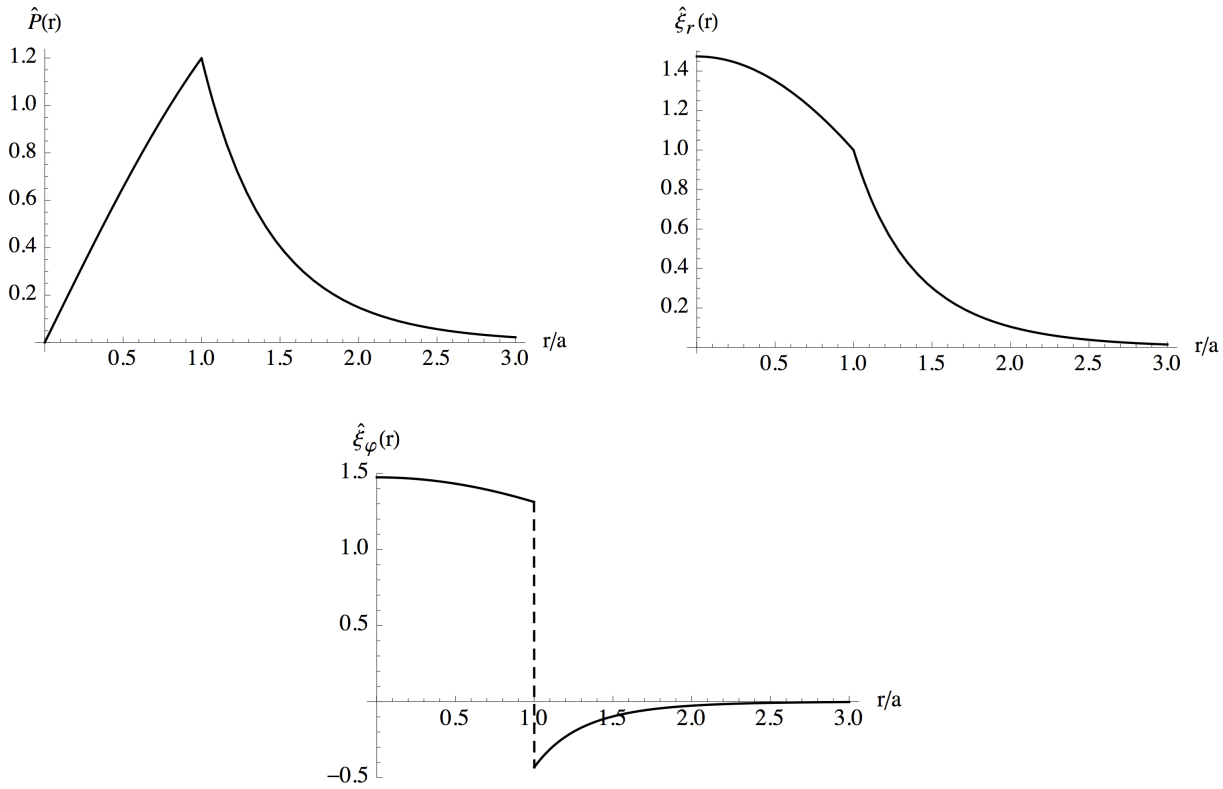

Figure 3.6: Perturbed pressure and displacement vector for ka=2, which corresponds to the longitudinal wavelength $\lambda = \pi a$. The eigenfunctions have been normalized so that the radial displacement is equal to one at the loop boundary ($r = a$).

In subsection 3.2 we imposed continuity of the perturbed pressure and the radial component of the displacement vector. Observing *Figures 3.5* and *3.6* we can verify that the continuity condition is satisfied. On the other hand, the azimuthal displacement has a discontinuity at the loop boundary $r = a$. Such a discontinuity is possible because the MHD equations impose no restriction on the behaviour of $\hat{\xi}_\varphi$ at the loop boundary. Furthermore, we can verify that the perturbed pressure and displacement vector vanish as $r \to \infty$.

The radial and azimuthal displacement components in *Figure 3.5* are constant for $r \leq a$. This implies that, for $ka = 0.1$, the entire cylinder moves as a rigid solid. In *Figure 3.6* these two functions are non-constant for $r \leq a$. Therefore, for $ka = 2$ any point of the cylinder moves with different radial and azimuthal velocity and, as a result, the internal density distribution changes in the course of the loop oscillations.

The perturbed pressure in both cases has a similar behaviour but in one of them it increases linearly for $r \leq a$ (*Figure 3.5*). This is caused by the cylinder behaving as a solid body for $ka = 0.1$. In the other case, the cylinder does not behave as a solid body so the perturbed pressure does not increase linearly (*Figure 3.6*).

In both cases, the azimuthal displacement has a discontinuity and a sign change at $r = a$. This fact means that at the loop boundary the interior and exterior particles are moving in opposite directions. Hence, there is a velocity shear at the loop boundary.

3.6.2. Region 2

In the second region, $k\, v_{Ae} < \omega$, there is a continuous of solutions. As in the first region, we chose a normalization such that $\hat{\xi}_r(r)$ equals one at the loop boundary ($r = a$). We then obtain

$$C_{1e} = \frac{\rho_0\, v_A^2\, k_i}{J'_m(k_i a)}. \tag{3.52}$$

Then the other two constants are

$$\begin{cases} C_{1i} = \rho_0\, v_A^2\, \dfrac{k_i \dfrac{J_m(k_i a)}{J'_m(k_i a)} - k_e \dfrac{J_m(k_e a)}{J'_m(k_e a)}}{Y_m(k_e a) - Y'_m(k_e a)\dfrac{J_m(k_e a)}{J'_m(k_e a)}}, & (3.53) \\ C_{2e} = \rho_0\, v_A^2\, \dfrac{k_i \dfrac{J_m(k_i a)}{J'_m(k_i a)} - k_e \dfrac{Y_m(k_e a)}{Y'_m(k_e a)}}{J_m(k_e a) - J'_m(k_e a)\dfrac{Y_m(k_e a)}{Y'_m(k_e a)}}. & (3.54) \end{cases}$$

Using the definitions (3.52), (3.53) and (3.54) the pressure in this frequency region can be expressed as follows

$$\hat{P}(r) = \begin{cases} C_{1i}\, J_m(k_i r), & r \le a, \quad (3.55) \\ C_{1e}\, J_m(k_e r) + C_{2e}\, Y_m(k_e r), & r > a. \quad (3.56) \end{cases}$$

Given that in this case there is a continuous of solutions, we can represent the pressure (3.55 and 3.56) and the radial (3.27) and azimuthal (3.29) components of the displacement vector for any value of ω and k satisfying $k\, v_{Ae} < \omega$. They are plotted in the following figures for the same parameter values as before and for three different values of k and ω.

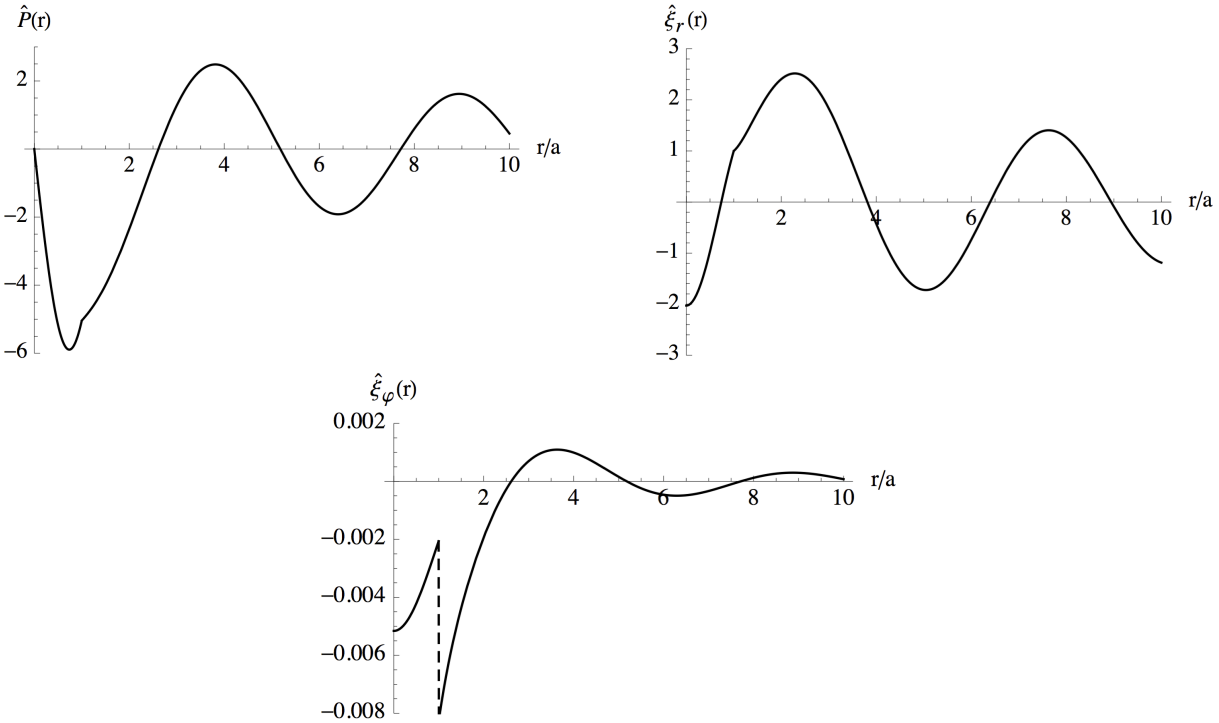

Figure 3.7: Perturbed pressure and displacement vector for ka=0.1 and $\omega a/v_{Ai} = 2.5$. The eigenfunctions have been normalized so that the radial displacement is equal to one at the loop boundary ($r = a$).

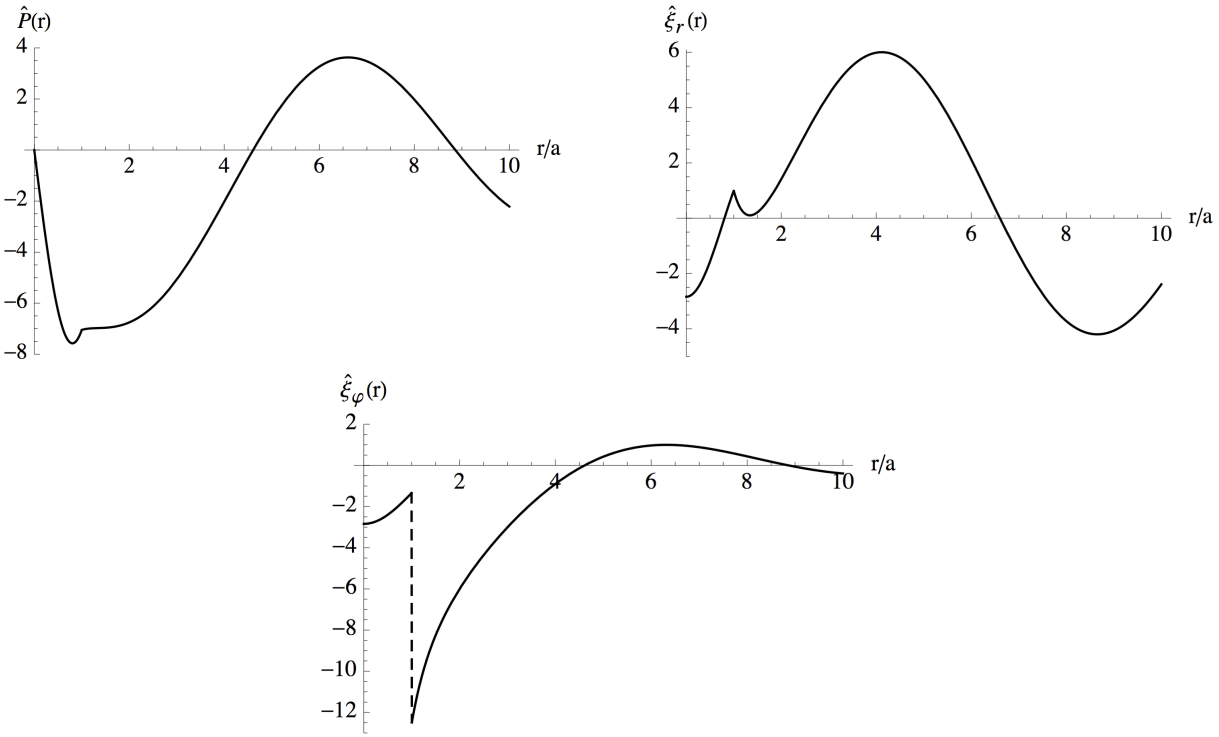

Figure 3.8: Same as *Figure 3.7* for ka=1 and $\omega a/v_{Ai} = 2.5$.

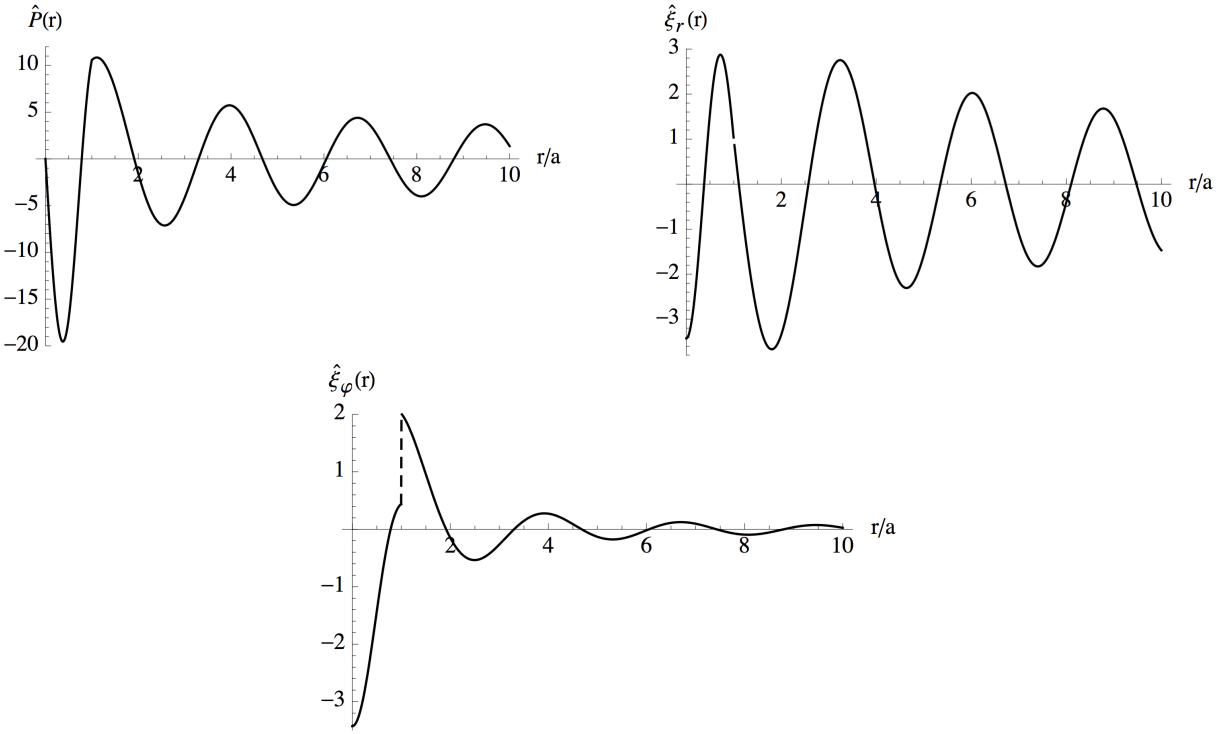

Figure 3.9: Same as *Figure 3.7* for ka=1 and $\omega a/v_{Ai} = 5$.

In the three *Figures 3.7, 3.8* and *3.9* the continuity condition on the perturbed pressure and the radial component of the displacement vector imposed in subsection 3.2 is satisfied. Furthermore, in the three cases the angular displacement has a discontinuity in $r = a$, which produces a velocity shear at the loop boundary. Moreover, all the functions are radially oscillatory in the loop environment because of their dependence on the Bessel functions *J* and *Y*.

The quantity κ_e plays the role of the radial wavenumber. For the values of k and ω used in *Figures 3.7, 3.8* and *3.9* we obtain respectively $\kappa_e a = 1.25, 0.75$ and 2.29. The smallest (largest) of these three values corresponds to *Figure 3.8* (*3.9*), which presents the longest (shortest) radial wavelength.

4. Linear Wave Energy

In this section we analyze the wave energy density, given by the sum of kinetic and magnetic energy densities. We also obtain expressions for the average of the wave energy over one period, one wavelength and one full turn around the cylinder. In order to interpret the solutions we finally plot the results. The material in this section is partly based on Goossens et al. (2013) and Moreels et al. (2015).

4.1. Energy equation

We follow Walker (2005) and write the energy equation as

$$\frac{\partial W}{\partial t} + \nabla \cdot \boldsymbol{Q} = 0, \tag{4.1}$$

where $W(\boldsymbol{r}, t)$ is the wave energy density and $\boldsymbol{Q}(\boldsymbol{r}, t)$ is the wave energy flux. These quantities are defined as

$$\begin{cases} W = \frac{1}{2}\rho_0 v^2 + \frac{p^2}{2\rho_0 c_s^2} - \left(\frac{1}{2c_s^2} g^2 \rho_0 + \frac{1}{2} g \frac{d\rho_0}{dz}\right) \xi_z^2 + \frac{B^2}{2\mu_0}, & (4.2) \\ \boldsymbol{Q} = p\boldsymbol{v} + \frac{1}{\mu_0} \boldsymbol{B} \times \boldsymbol{E}. & (4.3) \end{cases}$$

Furthermore, the velocity at which wave energy propagates is defined as the ratio of the above two quantities

$$\boldsymbol{R} = \frac{\boldsymbol{Q}}{W}. \tag{4.4}$$

The meaning of the terms in the wave energy density (4.2) is

- Kinetic energy density

$$KE = \frac{1}{2}\rho_0 \boldsymbol{v}^2, \tag{4.5}$$

- Magnetic energy density

$$ME = \frac{\boldsymbol{B}^2}{2\mu_0}, \tag{4.6}$$

- Pressure (or internal) energy density

$$IE = \frac{p^2}{2\rho_0 c_s^2}, \tag{4.7}$$

- Energy density associated to gravitational field

$$GE = -\left(\frac{1}{2c_s^2} g^2 \rho_0 + \frac{1}{2} g \frac{d\rho_0}{dz}\right) \xi_z^2. \tag{4.8}$$

In our treatment of the equilibrium and wave propagation we have neglected the plasma pressure and gravity in the momentum and energy equations so that we will neglect the last two energy density terms, (4.7) and (4.8). Therefore, we will consider the wave energy density as the sum of kinetic and magnetic energy density

$$W(r, z, \varphi, t) = KE(\boldsymbol{r}, t) + ME(\boldsymbol{r}, t) = \frac{1}{2}\rho_0 \boldsymbol{v}^2 + \frac{\boldsymbol{B}^2}{2\mu_0}. \tag{4.9}$$

4.2. Averaged wave energy density

We will compute the average of the wave energy over one period (T), one wavelength (λ) and one full turn around the cylinder (2π)

$$\langle W \rangle(r) = \frac{1}{2\pi T \lambda} \int_0^T \int_0^\lambda \int_0^{2\pi} W(r, z, \varphi, t) dt\, dz\, d\varphi. \tag{4.10}$$

Perturbed quantities $\left(\xi_r, \xi_\varphi, B_r, B_\varphi, B_z, \dots\right)$ have the general form $f(\boldsymbol{r}, t) = f_0(\boldsymbol{r}) + f_1(\boldsymbol{r}, t)$ given by expression (3.23) where only the real part of $f_1(\boldsymbol{r}, t)$ is kept

$$Re(f_1) = \frac{1}{2}(f_1 + {f_1}^*) = \frac{1}{2}\left(\hat{f}(r) e^{i\phi} + \hat{f}^*(r) e^{-i\phi}\right), \tag{4.11}$$

with $\phi = -\omega t + m\varphi + kz$. Both KE and ME contain squares of perturbed variables, which can be written as

$$(f_0 + Re(f_1))^2 = f_0^2 + 2 f_0 Re(f_1) + Re(f_1)^2, \tag{4.12}$$

where

$$\left(Re(f_1)\right)^2 = \frac{1}{4}\left(\hat{f}^2 e^{2i\phi} + {\hat{f}^*}^2 e^{-2i\phi} + 2\hat{f}\hat{f}^*\right). \tag{4.13}$$

Therefore, when averaging the kinetic and magnetic energy density, we will have integrals with the following general forms

$$\frac{1}{2\pi T\lambda}\int_0^T\int_0^\lambda\int_0^{2\pi} f_0 Re(f_1)dt\,dz\,d\varphi =$$

$$= \frac{1}{2}f_0\int_0^T\int_0^\lambda\int_0^{2\pi}\left(\hat{f}(r)e^{i\phi}+\hat{f}^*(r)e^{-i\phi}\right)dt\,dz\,d\varphi = 0, \tag{4.14}$$

$$\frac{1}{2\pi T\lambda}\int_0^T\int_0^\lambda\int_0^{2\pi}\left(Re(f_1)\right)^2 dt\,dz\,d\varphi =$$

$$= \frac{1}{2\pi T\lambda}\frac{\hat{f}(r)\hat{f}^*(r)}{2}\int_0^T\int_0^\lambda\int_0^{2\pi} dt\,dz\,d\varphi = \frac{\hat{f}(r)\hat{f}^*(r)}{2}, \tag{4.15}$$

where we have used that the integrals of terms proportional to $e^{\pm i\phi}$ or $e^{\pm 2i\phi}$ are zero.

Then, the average of the kinetic energy density, given by equation (4.5), is

$$\langle KE\rangle(r) = \frac{1}{4}\rho_o\hat{\boldsymbol{v}}\cdot\hat{\boldsymbol{v}}^*. \tag{4.16}$$

Using expressions (2.7) and (3.5) the kinetic energy density averaged can be written as follows

$$\langle KE\rangle(r) = \frac{1}{4}\rho_o\omega^2\hat{\boldsymbol{\xi}}\cdot\hat{\boldsymbol{\xi}}^*. \tag{4.17}$$

Assuming that the magnetic field has the general form (3.23) and using equations (3.13) and (3.16) we can express it as

$$\boldsymbol{B} = B_r\hat{e}_r + B_\varphi\,\hat{e}_\varphi + (B_0 + B_z)\,\hat{e}_z, \tag{4.18}$$

where $B_r = ikB_0\xi_r$, $B_\varphi = ikB_0\xi_\varphi$ and $B_z = \frac{P\mu_0}{B_0}$. Therefore, the average of the magnetic energy density, given by equation (4.6), is

$$\langle ME\rangle(r) = \frac{1}{2\pi T\lambda}\int_0^T\int_0^\lambda\int_0^{2\pi}\frac{1}{2\mu_0}\left(B_r^2 + B_\varphi^2 + B_z^2 + B_0^2 + 2B_0B_z\right)dt\,dz\,d\varphi. \tag{4.19}$$

Using the general results of the integrals (4.14) and (4.15) the magnetic energy density averaged can be written as

$$\langle ME\rangle(r) = \frac{1}{2\mu_0}\left(\frac{k^2B_0^2}{2}\hat{\xi}_r\hat{\xi}_r^* + \frac{k^2B_0^2}{2}\hat{\xi}_\varphi\hat{\xi}_\varphi^* + \frac{{\mu_0}^2}{2B_0^2}\hat{P}\hat{P}^* + B_0^2\right), \tag{4.20}$$

where the term $B_0^2/2\mu_0$ is the equilibrium magnetic energy density. Here we analyse the wave energy density and so this term can be dropped. Furthermore, assuming $\hat{\xi}_z = 0$, so that $\hat{\xi}_r\hat{\xi}_r^* + \hat{\xi}_\varphi\hat{\xi}_\varphi^* = \hat{\boldsymbol{\xi}} \cdot \hat{\boldsymbol{\xi}}^*$, the magnetic energy density is

$$\langle ME \rangle(r) = \frac{B_0^2}{4\mu_0}\left(k^2\hat{\boldsymbol{\xi}} \cdot \hat{\boldsymbol{\xi}}^* + \frac{{\mu_0}^2}{B_0^4}\hat{P}\hat{P}^*\right). \tag{4.21}$$

And using the equation (2.9) we finally obtain

$$\langle ME \rangle(r) = \frac{\rho_0 v_A^2}{4}\left(k^2\hat{\boldsymbol{\xi}} \cdot \hat{\boldsymbol{\xi}}^* + \frac{1}{(\rho_0 v_A^2)^2}\hat{P}\hat{P}^*\right). \tag{4.22}$$

The average of the total wave energy density is the sum of the kinetic (4.15) and magnetic (4.20) energy density averaged

$$\langle W \rangle(r) = \frac{1}{4}\left(\rho_0(\omega^2 + v_A^2 k^2)\,\hat{\boldsymbol{\xi}} \cdot \hat{\boldsymbol{\xi}}^* + \frac{1}{\rho_0 v_A^2}\hat{P}\hat{P}^*\right). \tag{4.23}$$

In order to simplify the calculations we define the kinetic and magnetic energy densities as dimensionless functions of dimensionless variables, which have been defined in *Table 3.2.* $\langle KE \rangle(r)$ and $\langle ME \rangle(r)$ can be written as functions of dimensionless variables as follows

$$\langle KE \rangle(r) = \frac{1}{4}\bar{\rho}_0\rho_i\bar{\omega}^2 v_{Ai}^2\left(\bar{\hat{\xi}}_r\bar{\hat{\xi}}_r^* + \bar{\hat{\xi}}_\varphi\bar{\hat{\xi}}_\varphi^*\right), \tag{4.24}$$

$$\langle ME \rangle(r) = \frac{\rho_0 v_A^2}{4}\left(\bar{k}^2\left(\bar{\hat{\xi}}_r\bar{\hat{\xi}}_r^* + \bar{\hat{\xi}}_\varphi\bar{\hat{\xi}}_\varphi^*\right) + \bar{\hat{P}}\bar{\hat{P}}^*\right). \tag{4.25}$$

The dimensionless functions can be obtained as shown in *Table 3.2.*

$$\overline{\langle KE \rangle}(\bar{r}) = \frac{1}{4}\bar{\rho}_0\bar{\omega}^2\left(\bar{\hat{\xi}}_r\bar{\hat{\xi}}_r^* + \bar{\hat{\xi}}_\varphi\bar{\hat{\xi}}_\varphi^*\right), \tag{4.26}$$

$$\overline{\langle ME \rangle}(\bar{r}) = \frac{1}{4}\left(\bar{k}^2\left(\bar{\hat{\xi}}_r\bar{\hat{\xi}}_r^* + \bar{\hat{\xi}}_\varphi\bar{\hat{\xi}}_\varphi^*\right) + \bar{\hat{P}}\bar{\hat{P}}^*\right), \tag{4.27}$$

$$\overline{\langle W \rangle}(\bar{r}) = \frac{1}{4}\left(\left(\bar{\rho}_0\bar{\omega}^2 + \bar{k}^2\right)\left(\bar{\hat{\xi}}_r\bar{\hat{\xi}}_r^* + \bar{\hat{\xi}}_\varphi\bar{\hat{\xi}}_\varphi^*\right) + \bar{\hat{P}}\bar{\hat{P}}^*\right). \tag{4.28}$$

Finally, using the expression of the pressure of the discrete mode, (3.50) and (3.51), and the definition of the displacement vector, (3.27) and (3.29), the kinetic and magnetic energies can be expressed as

$$\overline{\langle KE\rangle}(\bar{r}) = \begin{cases} \dfrac{\bar{\rho}_i\bar{\omega}^2}{4\,J_m'^{\,2}(\bar{k}_i\bar{a})}\left(J_m'^{\,2}(\bar{k}_i\bar{r}) + \dfrac{m^2}{\bar{r}^2\bar{k}_i^2}J_m^2(\bar{k}_i\bar{r})\right), & \bar{r}\le 1, \quad (4.29) \\ \dfrac{\bar{\rho}_e\bar{\omega}^2}{4\,K_m'^{\,2}(\bar{\kappa}_e\bar{a})}\left(K_m'^{\,2}(\bar{\kappa}_e\bar{r}) + \dfrac{m^2}{\bar{r}^2\bar{\kappa}_e^2}K_m^2(\bar{\kappa}_e\bar{r})\right), & \bar{r}>1. \quad (4.30) \end{cases}$$

$$\overline{\langle ME\rangle}(\bar{r}) = \begin{cases} \dfrac{1}{4\,J_m'^{\,2}(\bar{k}_i\bar{a})}\left(\bar{k}^2\,J_m'^{\,2}(\bar{k}_i\bar{r}) + \left(\dfrac{m^2\bar{k}^2}{\bar{r}^2\bar{k}_i^2} + \bar{k}_i^2\right)J_m^2(\bar{k}_i\bar{r})\right), & \bar{r}\le 1, \quad (4.31) \\ \dfrac{1}{4\,K_m'^{\,2}(\bar{\kappa}_e\bar{a})}\left(\bar{k}^2K_m'^{\,2}(\bar{\kappa}_e\bar{r}) + \left(\dfrac{m^2\bar{k}^2}{\bar{r}^2\bar{\kappa}_e^2} + \bar{\kappa}_e^2\right)K_m^2(\bar{\kappa}_e\bar{r})\right), & \bar{r}>1. \quad (4.32) \end{cases}$$

4.3. Results

We compute the energy density of the fundamental discrete (proper) mode, whose eigenfunctions have been shown in *Figures 3.5* and *3.6* for two different longitudinal wavelengths. Continuous (improper) modes have eigenfunctions that are non-square integrable and for this reason their energy density integrated over the whole spatial domain is infinite.

4.3.1. Radial variation of the energy density

In the following figures we plot the radial variation of the kinetic and magnetic energy densities given by equations (4.29), (4.30), (4.31) and (4.32) for the parameter values used before, namely $\rho_e/\rho_i = 1/4$ and $m = 1$.

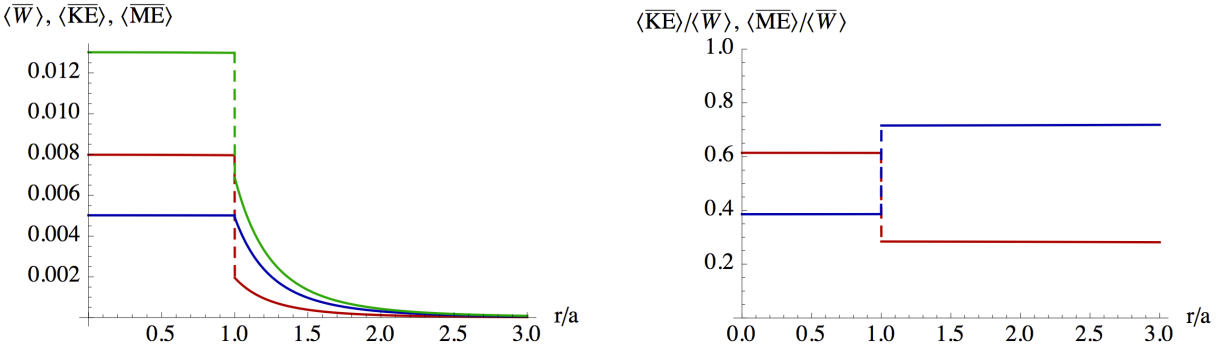

Figure 4.1: Radial dependence of the total (green), kinetic (red) and magnetic (blue) energy density for the eigenmode of *Figure 3.5* ($\bar{k} = 0.1$). Left: energy densities. Right: energy densities normalized to the total energy density.

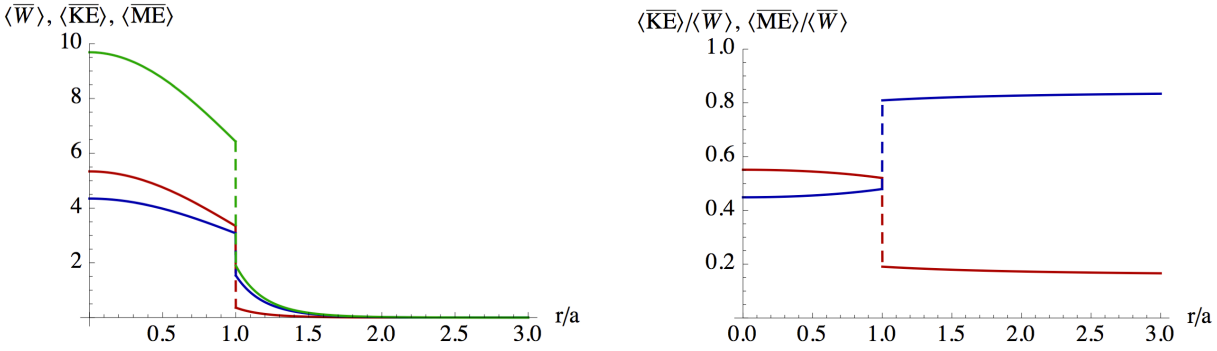

Figure 4.2: Same as *Figure 4.1* for the eigenmode of *Figure 3.6* ($\bar{k} = 2$).

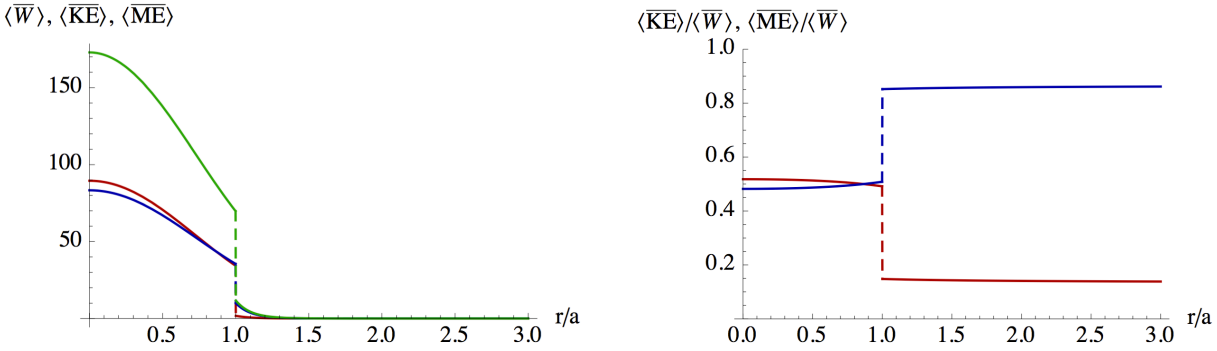

Figure 4.3: Same as *Figure 4.1* for the eigenmode with $\bar{k} = 5$.

We first make a comparison of the radial distribution of the kinetic and magnetic energy densities. In the left panel one can appreciate that most of the energy is concentrated inside the coronal loop, where the kinetic contribution is dominant over the magnetic one. Furthermore, outside the loop the magnetic energy is more important and both terms decay quickly with r.

The right panel in *Figure 4.1* shows that the energy percentage associated to the kinetic and magnetic terms is independent of r both inside and outside the cylinder: their respective contributions are roughly 60% and 40% inside the loop and 30% and 70% outside the loop. Increasing $\bar{k}$ (*Figures 4.2* and *4.3*) leads to the total energy being more evenly distributed between kinetic and magnetic inside the loop and less evenly distributed in the environment. Inside the loop and in the limit of $\bar{k} \to \infty$ the two energies become equal because the pressure term, which appears in the magnetic energy, vanishes. In this case we would have energy equipartition. *Figure 4.3* provides a hint of this behaviour of the energy densities as $\bar{k} \to \infty$.

The kinetic energy density for $r \leq a$ and $\bar{k} = 0.1$ (*Figure 4.1*) behaves as constant because the loop moves as a solid body. On the other hand, for the values $\bar{k} = 2$ (*Figure 4.2*) or $\bar{k} = 5$ (*Figure 4.3*) we can observe that the kinetic energy density does not have a constant value for $\bar{r} \leq 1$. Hence, for these values of $\bar{k}$ any point of the loop has a different velocity and also different kinetic and magnetic energies.

In the three cases we have studied the kinetic energy density is bigger than the magnetic energy density for small values of r/a, but there is a point where the magnetic

term exceeds the kinetic one. In *Figures 4.1* and *4.2* this point is at the loop boundary $r/a = 1$ and in *Figure 4.3* it is inside the loop. This is very clearly seen in the crossing of the red and blue curves on the right panel of *Figure 4.3*. The reason for this behaviour is beyond the scope of this work.

4.3.2. Variation of the energy density with the longitudinal wavenumber

Here we integrate $\langle KE\rangle(r)$ and $\langle ME\rangle(r)$ over the interval $0 < r < \infty$ to obtain the energy densities over the whole volume. The general form of those integrals is

$$\langle W\rangle = \int_0^\infty \langle W\rangle(r)\ r\ dr = \int_0^a \langle W_i\rangle(r)\, r\, dr + \int_a^\infty \langle W_e\rangle(r)\, r\, dr, \tag{4.33}$$

where $\langle W_i\rangle(r)$ and $\langle W_e\rangle(r)$ refer to the total energy density as a function of position inside and outside the cylinder.

Using the dimensionless expressions (4.29) and (4.30) for the kinetic and (4.31) and (4.32) for the magnetic energies and applying the general form (4.33) we have the following

$$\overline{\langle KE\rangle} = \frac{\bar\rho_i \bar\omega^2}{4\, {J'_m}^2(\bar k_i \bar a)}\left(\int_0^{\bar a} {J'_m}^2(\bar k_i r)\, r\, dr + \frac{m^2}{\bar k_i^2}\int_0^{\bar a} J_m^2(\bar k_i r)\frac{1}{r}\, dr\right) + \frac{\bar\rho_e \bar\omega^2}{4\, {K'_m}^2(\bar\kappa_e \bar a)}\left(\int_{\bar a}^\infty {K'_m}^2(\bar\kappa_e r)\, r\, dr + \frac{m^2}{\bar\kappa_e^2}\int_{\bar a}^\infty K_m^2(\bar\kappa_e r)\frac{1}{r}\, dr\right), \tag{4.34}$$

$$\overline{\langle ME\rangle} = \frac{1}{4\, {J'_m}^2(\bar k_i \bar a)}\left(\bar k^2\int_0^{\bar a} {J'_m}^2(\bar k_i r)\, r\, dr + \frac{m^2\bar k^2}{\bar k_i^2}\int_0^{\bar a} J_m^2(\bar k_i r)\frac{1}{r}\, dr + \bar k_i^2\int_0^{\bar a} {J_m}^2(\bar k_i r)\, r\, dr\right) + \frac{1}{4\, {K'_m}^2(\bar\kappa_e \bar a)}\left(\bar k^2\int_{\bar a}^\infty {K'_m}^2(\bar\kappa_e r)\, r\, dr + \frac{m^2\bar k^2}{\bar\kappa_e^2}\int_{\bar a}^\infty K_m^2(\bar\kappa_e r)\frac{1}{r}\, dr + \bar\kappa_e^2\int_{\bar a}^\infty {K_m}^2(\bar\kappa_e r)\, r\, dr\right). \tag{4.35}$$

If we assume $m = 1$, which corresponds to the fundamental discrete kink mode, the integrals of Bessel's functions that appear in the above expressions can be solved using the primitives given in Rosenheinrich (2014), pp. 166 and 185. Therefore, the dimensionless kinetic and magnetic energy densities of the fundamental discrete mode as a function of the linear wavenumber are

$$\overline{\langle KE\rangle} = \frac{\bar\rho_i \bar\omega^2}{8\,\bar k_i^2 {J'_1}^2(\bar k_i \bar a)}\left(\left(\bar k_i \bar a\right)^2 J_0^2(\bar k_i \bar a) + \left(\left(\bar k_i \bar a\right)^2 - 2\right)J_1^2(\bar k_i \bar a)\right) + \frac{\bar\rho_e \bar\omega^2}{8\,{\bar\kappa_e}^2 {K'_1}^2(\bar\kappa_e \bar a)}\left((\bar\kappa_e \bar a)^2 + 1)K_1^2(\bar\kappa_e \bar a) - ((\bar\kappa_e \bar a)^2 + 2)K_0^2(\bar\kappa_e \bar a)\right), \tag{4.36}$$

$$\overline{\langle ME\rangle} = \frac{1}{8\,\bar{k}_i^2 J_1'^2(\bar{k}_i\bar{a})}\Big(\bar{k}^2\left[(\bar{k}_i\bar{a})^2 J_0^2(\bar{k}_i\bar{a}) + \left((\bar{k}_i\bar{a})^2 - 2\right)J_1^2(\bar{k}_i\bar{a})\right] + \bar{k}_i^4\bar{a}\left[\bar{a}\left(J_0^2(\bar{k}_i\bar{a}) + J_1^2(\bar{k}_i\bar{a})\right) - 2J_0^2(\bar{k}_i\bar{a})J_1^2(\bar{k}_i\bar{a})\right]\Big) + \frac{1}{8\,\bar{\kappa}_e^2 K_1'^2(\bar{\kappa}_e\bar{a})}\Big(\bar{k}^2[((\bar{\kappa}_e\bar{a})^2+2)K_1^2(\bar{\kappa}_e\bar{a}) - ((\bar{\kappa}_e\bar{a})^2+1)K_0^2(\bar{\kappa}_e\bar{a})] - \bar{\kappa}_e^4\bar{a}\left[\bar{a}\left(K_1^2(\bar{\kappa}_e\bar{a}) - K_0^2(\bar{\kappa}_e\bar{a})\right) + 2K_0(\bar{\kappa}_e\bar{a})K_1(\bar{\kappa}_e\bar{a})\right]\Big). \quad (4.37)$$

Finally, in *Figure 4.4* we plot the kinetic (4.36) and magnetic (4.37) energy densities for the parameter values used before, namely $\rho_e/\rho_i = 1/4$ and $m = 1$. This is done for longitudinal wavenumbers $0 < \bar{k} < 5$ so that the influence of the wavenumber can be clearly appreciated.

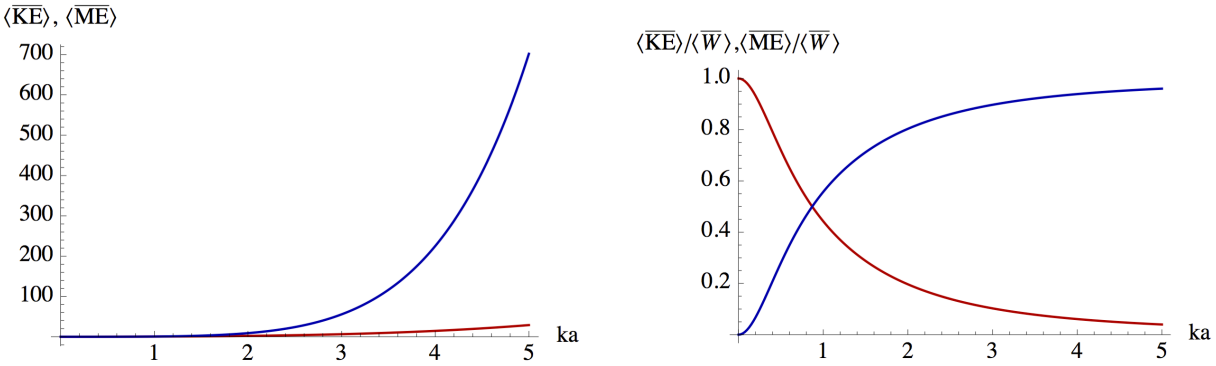

Figure 4.4: Left: kinetic (red) and magnetic (blue) energy density of the fundamental discrete kink mode as a function of wavenumber. Right: percentage of the total energy associated to the kinetic and magnetic terms for the fundamental discrete kink mode

In the left panel of *Figure 4.4* we can observe that, for the constants C_{1i} and C_{4e} chosen here, the total kinetic and magnetic energy densities increase with the longitudinal wavenumber. Furthermore, for wavenumbers values larger than *2*, the magnetic energy density increases much faster than the kinetic one.

In the right panel of *Figure 4.4* we show the percentage of each energy density. For wavenumber values $\bar{k} < 1$ the kinetic energy dominates over the magnetic one. On the other hand, for values $\bar{k} > 1$ the magnetic energy becomes much larger than the kinetic one, which becomes negligible.

Conclusions

This project has been focused on magnetohydrodynamic waves in solar coronal loops, studying the total pressure and displacement vector behaviour depending on the value of the longitudinal wavenumber. The wave energetics has also been investigated.

We have considered a coronal loop in static equilibrium, modelled as a straight magnetic cylinder, which we have perturbed about the equilibrium state. Introducing the perturbed quantities in the MHD equations and imposing the continuity of the pressure and the radial displacement at the loop boundary, we have obtained expressions for the radial variation of the perturbed pressure and displacement vector. These solutions have been found in three different frequency regions, depending on the value of the quantity k_r^2, where k_r plays the role of a radial wavenumber.

Some plots have been included to interpret the physical nature of these solutions for the $m = 1$ case. We have realised that for small values of the longitudinal wavenumber (e.g., $ka = 0.1$), in the frequency region $k\, v_{Ai} < \omega < k\, v_{Ae}$, the coronal loop behaves as a solid body. Moreover, both in this frequency region and for $k\, v_{Ae} < \omega$, for which we have allowed values of the frequency, a velocity shear at the loop boundary is present. Furthermore, in the frequency region $k\, v_{Ae} < \omega$, we have shown that the pressure and displacement vector in the loop environment possess a radially oscillatory behaviour because of their dependence on the Bessel functions *J* and *Y*.

In the last section we have analyzed the radial variation of the kinetic and magnetic energy densities for different values of the longitudinal wavenumber in the frequency region $k\, v_{Ai} < \omega < k\, v_{Ae}$. We have shown that most of the energy density is concentrated inside the coronal loop, where the kinetic contribution is dominant over the magnetic one. Outside the loop, where the magnetic contribution is more important, both energy densities decay rapidly with r. Furthermore, we have shown that increasing the longitudinal wavenumber the total energy becomes more evenly distributed between kinetic and magnetic inside the loop and less evenly distributed in the environment. Moreover, inside the loop and in the limit $k \to \infty$ we have energy equipartition.

Finally, we have obtained the energy densities over the whole volume as a function of the longitudinal wavenumber. We have shown that these total energy densities increase with the longitudinal wavenumber and that, for values of $ka > 2$, the magnetic energy density increases much faster than the kinetic one.

For future projects it would be interesting to study the case in which the azimuthal wavenumber is $m \neq 1$ and also the superposition of two waves of equal amplitude travelling in opposite directions. The wave energy flow, represented by the vector $\boldsymbol{Q}$ in equation (4.1), is also worth being investigated. The energetics of improper modes could also be addressed.

It should be noted that the results we have obtained are approximations because (i) coronal loops have curvature and so are not perfect cylinders and (ii) we have assumed that perturbations are much smaller than their corresponding equilibrium values.

Bibliography

Canfield, R. (2001) "Solar Active Regions", Nature Publishing Group 2001.

Chen, F.F. (1984) "Plasma Physics and Controlled Fusion",2nd edition, Plenum Press.

Goedbloed, H. P. and Poedts, S. (2004) "Principles of Magnetohydrodynamics", Cambridge University Press, chapters 3 and 4.

Goossens, M., Van Doorsselaere, T., Soler, R. and Verth, G. (2013) "Energy content and propagation in transverse solar atmospheric waves", The Astrophysical Journal, **768**, 191 (12 pp.). 768.

Moreels, M. G., Van Doorsselaere, T., Grant, S. D. T., Jess, D. B. and Goossens, M. (2015) "Energy and energy flux in axisymmetric slow and fast waves", Astronomy & Astrophysics, **578**, A60 (14 pp.). 578.

Priest (2014) "Magnetohydrodynamics of the Sun", Cambridge University Press, chapter 2.

Rosenheinrich, W. (2015) "Tables of some indefinite integrals of Bessel functions" (http://www.fh-jena.de/~rsh/Forschung/Stoer/besint.pdf).

Ruderman, M. S. and Erdélyi, R. (2009) "Transversal Oscillations of Coronal Loops", Space Science Reviews, **149**, 199-228. 149.

Walker, A. (2005) "Magnetohydrodynamic Waves in Geospace. The Theory of ULF Waves and Their Interaction with Energetic Particles in the Solar-Terrestrial Environment", Institute of Physics Publishing, p. 175.

Web resources

http://apod.nasa.gov/apod/ap090726.html, Koen van Gorp.

https://www.spaceweatherlive.com/en/help/what-are-sunspots.

http://www.nasa.gov/sites/default/files/halloween_sun_2014_2k.jpg, NASA/SDO.

http://www.nasa.gov/centers/goddard/news/topstory/2008/coronal_loops.html, NASA/TRACE.